"a novel iterative finite-differencing scheme has been developed to solve nonlinear partial differential equations,"

Combined Forced and Free Convection in the Entrance Region of a Horizontal Pipe

by Morrison Sistuzo Montesclaros, B.S.M.E.

Abstract

The effect of buoyancy on laminar forced convection in the entrance region of a uniformly heated horizontal pipe, where the velocity and temperature fields are developing simultaneously, is investigated for the case of Gr = 5000. All of the terms of the time-dependent governing equations are taken into account so that the results obtained can be applied to low Prandtl number fluids for which the results obtained from large Prandtl number assumptions are no longer valid. A novel iterative method is developed to solve nonlinear partial differential equations, and has proven to ensure stability and faster rate of convergence. The developing primary and secondary velocity profiles, developing temperature field, and local and average Nusselt numbers are. presented to clarify the free convection effect. Values are compared with those obtained from pure forced convection.

Introduction

The importance of buoyancy effects on laminar heat transfer has led to many theoretical investigations on combined free and forced convection in horizontal or vertical tubes. For the case of horizontal tubes with uniform wall temperature, the free convection effect becomes very important only in the entrance region since the effect disappears as the bulk temperature approaches the wall temperature in the fully developed region. The equations of state for this problem are still very difficult to solve analytically so that numerical analysis using finite-difference techniques are used. Various studies [1-4] have been published, but with modifications of the governing equations. In short, numerical analysis to date on combined free and forced laminar convection in a horizontal tube has been made possible only by using the large

*Master of Engineering Thesis, Nagoya Institute of Technology, Nagoya, Japan.

**Member, Presidential Technical Staff, Cebu Institute of Technology.

Prandtl number assumption. Though the results are helpful in the understanding of the problem, they are practical only for large Prandtl number fluids. Some investigators [3,4] assume hydro-dynamically fully developed velocity fields, with emphasis only on the thermal entrance region. The results obtained from this assumption cannot satisfactorily describe the complex heat transfer phenomena in the entrance region where the velocity and temperature fields are developing simultaneously.

This research presents theoretical results of the effect free convection on laminar forced flow in the entrance region of a horizontal pipe with uniform wall temperature. A Prandtl number of 0.71 (air) is assumed to represent fluids for which the above-mentioned large Prandtl number assumption is no longer valid. For such a relatively small Prandtl number, the inertia terms in the momentum equations cannot be neglected, and so here all the terms in the time- dependent governing equations are taken into account. Physical properties are assumed constant except for the density which is temperature-dependent. Primitive variable (U,P) system is used in contrast to the commonly used vorticity-stream function (ω,ψ) system. The (ω,ψ) system is not practically effective to be used in three-dimensional problems. The difficulty lies in the assumption of appropriate boundary conditions. Ou and Cheng [4] used the verticity-stream function system, but the assumption that the main flow retained Poiseuille profile, unaffected by the secondary flow, reduced the problem into a two-dimensional flow wherein the (ω,ψ) system could be used to its greater advantage.

A novel iterative method is developed in this research to solve nonlinear partial differential equations. This method has proven to ensure stability and faster rate of convergence.

The developing primary and secondary velocity profiles, developing temperature fields, and local and average Nusselt numbers are presented to clarify the free convection effect.

Governing Equations

Consideration is given to a fluid in laminar forced flow with simultaneously developed velocity and thermal fields. The fluid is assumed incompressible with constant physical properties except for the density which is temperature dependent and important only in the buoyancy terms of the momentum equations. Viscous dissipation is neglected. The fluid enters the pipe with a uniform velocity w'_0 and at a uniform temperature t'_0. The horizontal, semi-infinite pipe is uniformly heated at a temperature t'_w. The cylindrical coordinate system is shown in Fig. A.

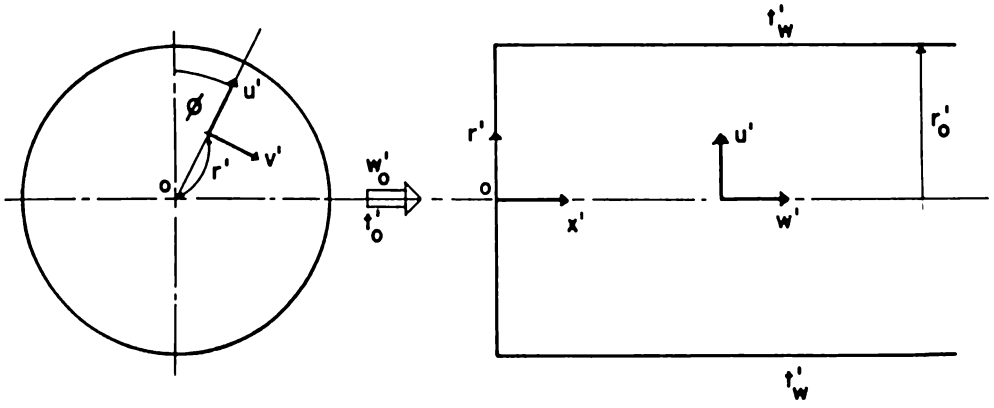

Fig. A. Cylindrical coordinate system.

The governing equations make use of the continuity, momentum, and energy equations [5]. With reference to the coordinate system shown in Fig. A, the full, three-dimensional, time-dependent equations are:

Continuity Equation

$$\frac{\partial(r'u')}{\partial r'} + \frac{\partial v'}{\partial \phi} + \frac{\partial(r'w')}{\partial x'} = 0 \qquad (1)$$

Momentum Equations

$$\frac{\partial u'}{\partial t'} + u'\frac{\partial u'}{\partial r'} + \frac{v'}{r'}\frac{\partial u'}{\partial \phi} + w'\frac{\partial u'}{\partial x'} - \frac{v'^2}{r'}$$

$$= -\frac{1}{\rho}\frac{\partial p'}{\partial r'} + \nu\left(\nabla^2 u - \frac{u'}{r'^2} - \frac{2}{r'^2} - \frac{\partial v'}{\partial \phi}\right)$$

$$- g\cos\phi \qquad (2)$$

$$\frac{\partial v'}{\partial t'} + u'\frac{\partial v'}{\partial r'} + \frac{v'}{r'}\frac{\partial v'}{\partial \phi} + w'\frac{\partial v'}{\partial x'} + \frac{u'v'}{r'}$$

$$= \frac{1}{\rho r'}\frac{\partial o'}{\partial \phi} + \nu\left(\nabla^2 v' + \frac{2}{r'^2}\frac{\partial u'}{\partial \phi} - \frac{v'}{r'^2}\right)$$

$$+ \; g \; \sin\phi \tag{3}$$

$$\frac{\partial w'}{\partial \tau'} + u' \frac{\partial w'}{\partial r'} + \frac{v'}{r'} \frac{\partial w'}{\partial \phi} + w' \frac{\partial w'}{\partial x'}$$

$$= - \frac{1}{\rho} \frac{\partial \rho'}{\partial x'} + \nu \nabla^2 w' \tag{4}$$

Energy Equation

$$\frac{\partial t'}{\partial \tau'} + u' \frac{\partial t'}{\partial r'} + \frac{v'}{r'} \frac{\partial t'}{\partial \phi} + w' \frac{\partial t'}{\partial x'} = \kappa \nabla^2 t' \tag{5}$$

Here, the Laplacean operator is defined:

$$\nabla^2 = \frac{\partial^2}{\partial r'^2} + \frac{1}{r'} \frac{\partial}{\partial r'} + \frac{1}{r'^2} \frac{\partial^2}{\partial \phi^2} + \frac{\partial^2}{\partial x'^2}$$

Let any point be a differential distance from the wall at temperature t' and density p. The small differences in temperature and density are given by:

$$\Delta t' = t' - t'_w$$

$$\Delta p = p - p_w$$

With the coefficient of volumetric expansion β given by

$$\beta = - \frac{\partial \rho w / \partial t'}{p_w} \quad ,$$

and the Boussinesq approximation for Δp given by

$$= \frac{\partial p_w}{\partial t'} t' \quad , \text{ we have}$$

$$\Delta p = - p_w \beta \Delta t'$$

Consider a point at pressure P_0 in a fluid at static condition with a uniform

temperature t'_w and density ρ_w. The equations for pressure deviations are given by:

$$\frac{\partial P_o}{\partial r'} = - \rho_w \, g \, \cos\phi$$

$$\frac{\partial P_o}{\partial \phi} = \rho_w \, g \, \sin\phi$$

$$\frac{\partial P_o}{\partial x'} = 0$$

Now let there be a density gradient $\Delta\rho$ which causes a pressure gradient P" on the point. With $P' = P_o + P''$, the equation for pressure deviation would then be:

$$\frac{1}{\rho} \frac{\partial P'}{\partial r'} = \frac{1}{\rho_w + \Delta\rho} \frac{\partial (P_o + P'')}{\partial r'}$$

$$= \frac{1}{\rho_w} (1 - \frac{\Delta\rho}{\rho_w}) (\frac{\partial P_o}{\partial r'} + \frac{\partial P''}{\partial r'})$$

$$= \frac{1}{\rho_w} \frac{\partial P_o}{\partial r'} - \frac{\Delta\rho}{\rho_w^2} \frac{\partial P_o}{\partial r'} + \frac{1}{\rho_w} \frac{\partial P''}{\partial r'}$$

and with Eq. (7).

$$\frac{1}{\rho} \frac{\partial P'}{\partial r'} = - g \cos\phi - \beta \, g \, \Delta t' \cos\phi + \frac{1}{\rho_w} \frac{\partial P''}{\partial r'}$$

Consequently, for the ϕ and x' directions:

$$\frac{1}{\rho r'} \frac{\partial P'}{\partial \phi} = g \sin\phi + \beta \, g \, \Delta t' \sin\phi + \frac{1}{\rho_w r'} \frac{\partial P''}{\partial \phi} \quad (9)$$

$$\frac{1}{\rho}\frac{\partial P'}{\partial x'} = \frac{1}{\rho_w}\frac{\partial P''}{\partial x'} \tag{10}$$

The following dimensionless numbers are introduced:

$$u = \frac{Re}{2}\frac{u'}{w_o'} \qquad v = \frac{Re}{2}\frac{v'}{w_o'} \qquad w = \frac{w'}{w_o'}$$

$$x = \frac{x'}{r_o'}\frac{2}{Re} \qquad r = \frac{r'}{r_o'} \qquad Re = \frac{2 r_o' w_o'}{\nu}$$

$$P = \frac{P''}{\rho w_0'/2} \qquad \theta = \frac{t' - t_w'}{t_o' - t_o'} \qquad Pr = \frac{\nu}{\kappa}$$

$$Gr = \frac{\beta g r_o'^3 (t_w' - t_o')}{\nu^2} \qquad \tau = \frac{2 w_o' t'}{Re r_o'}$$

With Eqs. (6), (8)-(10), and the above dimensionless numbers. Eqs. (2)-(5) could be written:

Continuity Equation

$$\frac{\partial (ru)}{\partial r} + \frac{\partial v}{\partial \phi} + \frac{\partial (rw)}{\partial x} = 0 \tag{11}$$

Momentum Equations

$$\frac{\partial u}{\partial \tau} + \frac{\partial u}{\partial r} + \frac{v}{r}\frac{\partial u}{\partial \phi} + w\frac{\partial u}{\partial x} - \frac{v^2}{r} \tag{12}$$

$$= -\frac{Re^2}{8}\frac{\partial P}{\partial r} + v^2 u - \frac{u}{r^2} - \frac{2}{r^2} - \frac{\partial v}{\partial \phi}$$

$$- Gr\ \theta\ \cos\phi$$

$$\frac{\partial v}{\partial t} + u\frac{\partial v}{\partial r} + \frac{v}{r}\frac{\partial v}{\partial \phi} + w\frac{\partial v}{\partial x} + \frac{uv}{r}$$

$$= -\frac{Re^2}{8}\frac{\partial P}{\partial \phi}\frac{1}{r} + \nabla^2 v + \frac{2}{r^2}\frac{\partial u}{\partial \phi} - \frac{v}{r^2} \qquad (13)$$

$$+ Gr\ \theta\ \sin\phi$$

$$\frac{\partial w}{\partial t} + u\frac{\partial w}{\partial r} + \frac{v}{r}\frac{\partial w}{\partial \phi} + w\frac{\partial w}{\partial x}$$

$$= -\frac{1}{2}\frac{\partial P}{\partial x} + \nabla^2 w \qquad (14)$$

Energy Equation

$$\frac{\partial \theta}{\partial t} + u\frac{\partial \theta}{\partial r} + \frac{v}{r}\frac{\partial \theta}{\partial \phi} + w\frac{\partial \theta}{\partial x} = \frac{1}{Pr}\nabla^2\theta \qquad (15)$$

Here, ∇^2 is the Laplacean operator defined:

$$\nabla^2 = \frac{\partial^2}{\partial r^2} + \frac{1}{r}\frac{\partial}{\partial r} + \frac{1}{r^2}\frac{\partial^2}{\partial \phi^2} + \frac{4}{Re^2}\frac{\partial^2}{\partial x^2}$$

The above equations are in the cylindrical coordinate system, and so, the center becomes a point of singularity. To solve for the velocities by numerical methods, we need finite values at the center. A transformation of variables is then introduced:

$$U = ru, V = rv, W = rw \qquad (16)$$

A transformation is also necessary to make the axial length finite. With c and m as positive constants,

$$X = 1 - \frac{1}{1 + (cx)^m} \tag{17}$$

With the above transformations, Eqs.(11)-(15) become:

$$\frac{\partial U}{\partial r} + \frac{1}{r}\frac{\partial V}{\partial \phi} + \frac{\partial W}{\partial X}\frac{dX}{dX} = 0 \tag{18}$$

$$\frac{\partial U}{\partial \tau} = -\frac{U}{r}\frac{\partial U}{\partial r} - \frac{V}{r^2}\frac{\partial U}{\partial \phi} - \frac{W}{r}\frac{\partial U}{\partial X}\frac{dX}{dx} + \frac{U^2}{r^2}$$

$$+ \frac{V^2}{r^2} - \frac{r}{2}\frac{Re^2}{4}\frac{\partial P}{\partial r} + \Delta^2 U - \frac{2}{r}\frac{\partial U}{\partial r}$$

$$- \frac{2}{r^2}\frac{\partial V}{\partial \phi} - r\ Gr\ \theta\ \cos\phi \tag{19}$$

$$\frac{\partial V}{\partial \tau} = -\frac{U}{r}\frac{\partial V}{\partial r} - \frac{V}{r^2} - \frac{\partial V}{\partial \phi} - \frac{W}{r}\frac{\partial V}{\partial X}\frac{dX}{dx}\frac{Re^2}{8}\frac{\partial P}{\partial \phi} \tag{20}$$

$$+ \Delta^2 V - \frac{2}{r}\frac{\partial v}{\partial r} + \frac{2}{r^2}\frac{\partial U}{\partial \phi} +$$

$$r\,G\,r\,\theta\,\sin\phi$$

$$\frac{\partial w}{\partial \tau} = -\frac{U}{r}\frac{\partial w}{\partial r} - \frac{V}{r^2}\frac{\partial w}{\partial \phi}\frac{W}{r}\frac{\partial w}{\partial x}\frac{dX}{dx} +$$

$$\frac{UW}{r^2}$$

$$- \frac{r}{2}\frac{\partial P}{\partial X}\frac{dX}{dX} + \nabla^2 W - \frac{2}{r}\frac{\partial W}{\partial r} + \frac{W}{r^2} \tag{21}$$

$$\frac{\partial \theta}{\partial \tau} = -\frac{U}{r}\frac{\partial \theta}{\partial r} - \frac{V}{r^2}\frac{\partial \theta}{\partial \phi} - \frac{W}{r}\frac{\partial \theta}{\partial X}\frac{dX}{dX} + \frac{1}{Pr}\nabla^2\theta \tag{22}$$

Here, the Laplacean operator ∇^2 is written:

$$\nabla^2 = \frac{\partial^2}{\partial r^2} + \frac{1}{r}\frac{\partial}{\partial r} + \frac{1}{r^2}\frac{\partial^2}{\partial \phi^2} + \frac{4}{Re^2}\left[\left(\frac{dx}{dx}\right)^2\frac{\partial^2}{\partial X^2} + \frac{d^2X}{dx^2}\frac{\partial}{\partial X}\right]$$

For the pressure field, an elliptic Poisson equation is used to ensure better results; and is given:

$$\nabla^2 P = -\frac{8}{Re^2}\left[\frac{1}{r}\frac{\partial}{\partial t}\left(\frac{\partial U}{\partial r}+\frac{1}{r}\frac{\partial V}{\partial \phi}+\frac{\partial W}{\partial X}\frac{dX}{dX}\right)\right.$$

$$+\ Gr\left(\cos\phi\frac{\partial \theta}{\partial r}-\frac{1}{r}\sin\phi\frac{\partial \theta}{\partial \phi}\right)+\frac{2}{r^4}(U^2+V^2)$$

$$-\frac{2}{r^3}U\frac{\partial U}{\partial r}+\frac{1}{r^2}\left(\frac{\partial U}{\partial r}\right)^2-\frac{2}{r^4}V\frac{\partial U}{\partial \phi}$$

$$+\frac{2}{r^3}\frac{\partial V}{\partial r}\frac{\partial U}{\partial \phi}-\frac{2}{r^3}W\frac{\partial U}{\partial X}\frac{dX}{dX}+\frac{1}{r^2}\left(\frac{\partial W}{\partial X}\right)^2\left(\frac{dX}{dx}\right)^2$$

$$+\frac{2}{r^2}\frac{\partial W}{\partial r}\frac{\partial U}{\partial X}\frac{dX}{dx}-\frac{2}{r^3}V\frac{\partial V}{\partial r}+\frac{2}{r^4}U\frac{\partial V}{\partial \phi}$$

$$\left.+\frac{1}{r^4}\left(\frac{\partial V}{\partial \phi}\right)^2+\frac{2}{r^3}\frac{\partial V}{\partial X}\frac{\partial W}{\partial \phi}\frac{dX}{dx}\right] \qquad (23)$$

Equation (23) has been derived using the continuity and momentum equations. (The detailed derivation is shown in the Appendix.). Equations (19)-(23) form the formal governing equations and are solved by iterative methods. The term in Eq. (23) which contains

$$\frac{\partial D}{\partial t},\ \left(D=\frac{\partial U}{\partial r}+\frac{1}{r}\frac{\partial V}{\partial \phi}+\frac{\partial W}{\partial X}\frac{dX}{dx}\right)$$

could easily have been cancelled out using the continuity equation. But because the Poisson equation is solved iteratively, the truncation error accumulates. The final result would not only be inaccuracy, but also nonlinear instability in the momentum equations. The inclusion of D could eliminate the nonlinear instability, as has been observed in many studies [6].

Boundary Conditions

The following are the boundary condition that are necessary for the given problem.

For The Velocity And Temperature Fields

(i) At the pipe inlet:

$u = v = O$, $w = 1$ (uniform flow)

$\Theta = 1$ (uniform entrance temperature)

(ii) At the infinite downstream:

$x = \infty$, $0 \leqslant r < 1$

$u = v = O$, $w = 2(1-r^2)$ (fully developed Poiseuille flow)

$\Theta = O$ (bulk temperature = wall temperature)

(iii) At the pipe wall:

$0 \leqslant x = \leqslant$, $r = 1$

$u = v = w = O$ (no slip condition)

$\Theta = O$ (uniform wall temperature)

(iv) At the vertical plane passing through the horizontal axis:

$0 \leqslant x \leqslant \infty$, $0 \leqslant r < 1$, $\phi = 0, \pi$

$v = O$ (symmetry)

The above boundary conditions are transformed according to Eqs. (16) and (17), to fit the governing equations. Hence,

(i) At the pipe inlet:

$$X = 0, \quad 0 \overset{\angle}{\equiv} r \angle 1$$

$$U = V = 0, \quad W = r, \quad \theta = 1$$

(ii) At the infinite downstream:

$$X = 1, \quad 0 \overset{\angle}{\equiv} r \angle 1$$

$$U = V = 0, \quad W = 2r(1 - r^2), \quad \theta = 0$$

(iii) At the pipe wall:

$$O \leqq X \leqq 1, \quad r = 1$$

$$U = V = W = O, \ \theta = O$$

(iv) At the vertical plane passing through the horizontal axis:

$$O \leqq X \leqq 1, \quad O \leqq r < 1, \quad \phi = O, \pi$$

$$V = O$$

For The Pressure Field

(i) At the pipe inlet:

$$x = O, \quad O \leqq r < 1$$

$$u = v = \frac{\partial u}{\partial x} = \frac{\partial^2 u}{\partial x^2} = O, \quad w = 1, \quad \theta = 1$$

With the above values, Eq. (12) gives:

$$\frac{\partial P}{\partial r} = - \frac{8}{Re^2} Gr \cos\phi$$

Therefore,

$$P = - \frac{8}{Re^2} r Gr \cos\phi + C(\phi) \cdot$$

At $r = O$, $P = P_{r=o}$ = constant ,

therefore,

$$P = P_{r=o} - \frac{8}{Re^2} r Gr \cos\phi \cdot$$

If we assume $P_{r=o} = \frac{8}{Re^2} Gr$, then

$$P = \frac{8}{Re^2} Gr (1 - r \cos\phi) \cdot$$

With Eq. (24), $\frac{1}{r}\frac{\partial P}{\partial \phi} = \frac{8}{Re^2}\ Gr \quad \sin\phi$ Gr $\sin\phi$ is obtained, which is identical to that obtained from Eq. (13) with the above boundary values. Therefore, the assumption $P_{r=o} = -\frac{8}{Re^2}$ Gr is valid.

(ii) At the infinite downstream:

$$x = \infty, \quad O \leqq r < 1$$

$$u = v = O, \quad w = 2(1-r^2), \quad \theta = O$$

$$\frac{\partial w}{\partial x} = \frac{\partial^2 w}{\partial x^2} = O, \quad \frac{\partial w}{\partial \phi} = \frac{\partial^2 w}{\partial \phi^2} = O$$

$$\frac{\partial P}{\partial x} = \text{constant}, \quad \frac{\partial P}{\partial r} = \frac{\partial P}{\partial \phi} = O$$

When these conditions are applied to Eqs. (12)-(14),

$$\frac{\partial P}{\partial x} = -16 \quad , \text{ hence,}$$

$$P = -16x + \text{constant}$$

Let the constant be P^* , then,

$$P = -16x + P^* \qquad (25)$$

With Eqs. (24) and (25), and the transformation in Eq. (17),

(i) At the pipe inlet:

$$X = O, \quad O \leqq r < 1$$

$$P^* = P = \frac{8}{Re^2}\ Gr(1-r\cos\phi)$$

(ii) At the infinite downstream:

$$X = 1, \quad O \leqq r < 1$$

$$P^* = \text{constant}$$

(iii) At the pipe wall:

$$r = 1, \quad O \leqq X \leqq 1$$

$$U = V = W = O, \quad \theta = O$$

With these conditions, Eq.(19) would give

$$\frac{\partial P}{\partial r} = \frac{8}{Re^2} \left(\frac{\partial^2 U}{\partial r^2} - \frac{\partial U}{\partial r} \right) \tag{26}$$

Using Taylor series expansion to approximate the derivatives at the wall,

$$\frac{\partial U}{\partial r} = \frac{3U_1 - 4U_2 + U_3}{2B} = \frac{-4U_2 + U_3}{2B}$$

$$\frac{\partial^2 U}{\partial r^2} = \frac{U_1 - 2U_2 + U_3}{B^2} = \frac{-2U_2 + U_3}{B^2}$$

Therefore Eq.(26) would give

$$\frac{\partial P}{\partial r} = \frac{8}{Re^2} \left(\frac{-2U_2 + U_3}{B^2} - \frac{-4U_2 + U_3}{2B} \right) \tag{27}$$

Equation (25) shows that the parameter P is infinitely decreasing. Since numerical analysis requires all the parameters to be finite, a transformation of P according to Eq.(25) is necessary before the governing equations could be used. When this transformation is applied, the governing equations would look just like those of Equations (19)-(23) with P^* instead of P, and a constant (+8) added to Eq.(21). For convenience in the finite-difference forms the symbol P is used instead of P^*. Thus, the final form of the governing equations would still be those of Equations (19)-(23), plus a constant 8 on the right-hand side of Eq.(21).

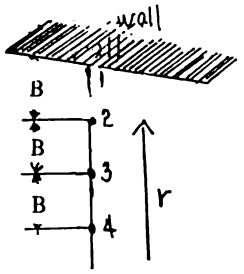

Fig. B

Finite-Difference Solution

Development of Equations

The governing equations are divided into three iterative loops, namely, the pressure loop, the temperature loop, and the velocity loop. In the pressure loop, Eq. (23), as iterations are done to evaluate convergent pressure values, the velocities do not change. Hence, ordinary space-centered differencing is used for the velocity derivatives while Euler's modified method is used for the first-order pressure derivatives, and Crank-Nicolson's method is used for the second-order pressure derivatives. Consequently, in the velocity loop, Eqs. (19)-(21), pressure derivatives are approximated by space-centered differencing while Euler's and Crank-Nicolson's methods are used for the velocities.

To illustrate the entire differencing scheme, an example is presented.

Take for example a nonlinear equation given below. (This model equation is fictitious and is used only for convenience in the presentation of the differencing scheme.)

$$\frac{\partial U}{\partial t} = -\frac{U}{r}\frac{\partial U}{\partial r} - \frac{V}{r^2}\frac{\partial V}{\partial \phi} - \frac{W}{r}\frac{\partial U}{\partial X} - \frac{r}{2}\frac{Re^2}{4}\frac{\partial P}{\partial r} + \frac{1}{r^2}\frac{\partial^2 U}{\partial \phi^2} \quad (28)$$

The finite-difference scheme would then be:

1. the first-order derivatives $\left(\frac{\partial U}{\partial r}, \frac{\partial V}{\partial \phi}, \frac{\partial U}{\partial X}\right)$ are approximated using Euler's modified method ([6] p. 84).

2. The second-order derivative $\frac{\partial^2 U}{\partial r^2}$ is evaluated using Crank-Nicolson's method [8].

3. The variables U, V, W are taken as constants whose values are of the previous time level.

4. The first-order derivative $\frac{\partial P}{\partial r}$ is evaluated by ordinary space-centered differencing, because the model equation is for the velocity evaluation in the velocity loop.

5. The firts-order derivative $\frac{\partial U}{\partial t}$ is approximated by forward-time differencing.
6. A point SOR (successive over-relaxation) method is then used for the entire equation [8].

With reference to Fig. C, which is used for convenience in the representation of node points, the finite-difference equation for the model equation is given:

$$\frac{U_e^{n+1} - U_e^n}{\Delta t} = -\frac{U_e^n}{r}\left[\frac{1}{2}\left(\frac{U_c^{n+1} - U_d^{n+1}}{2B} + \frac{U_c^n - U_d^n}{2B}\right)\right]$$

$$- \frac{V_e^n}{r^2}\left[\frac{1}{2}\left(\frac{V_f^{n+1} - V_g^{n+1}}{2\Delta\phi} + \frac{V_f^n - V_g^n}{2\Delta\phi}\right)\right]$$

$$- \frac{W_e^n}{r}\left[\frac{1}{2}\left(\frac{U_a^{n+1} - U_b^{n+1}}{2A} + \frac{U_a^{n+} - U_b^n}{2A}\right)\right]$$

$$- \frac{r}{2}\frac{Re^2}{4}\frac{P_c^n - P_d^n}{2B}$$

$$+ \frac{1}{r^2}\left[\frac{1}{2}\left(\frac{U_f^{n+1} + 2U_e^{n+1} + U_g^{n+1}}{\Delta\phi^2} - \frac{U_f^n + 2U_e^n + U_g^n}{\Delta\phi^2}\right)\right]$$

Let $C_1 = -\frac{U_e^n \Delta t}{r4B}$, $C_2 = -\frac{V_e^n \Delta t}{4\Delta\phi r^2}$, $C_3 = -\frac{W_e^n \Delta t}{r4A}$, $C_4 = -\frac{r}{2}\frac{Re^2 \Delta t}{8B}$

$C_5 = \frac{\Delta t}{2r^2\Delta\phi^2}$, so that Eq. (29) could be written;

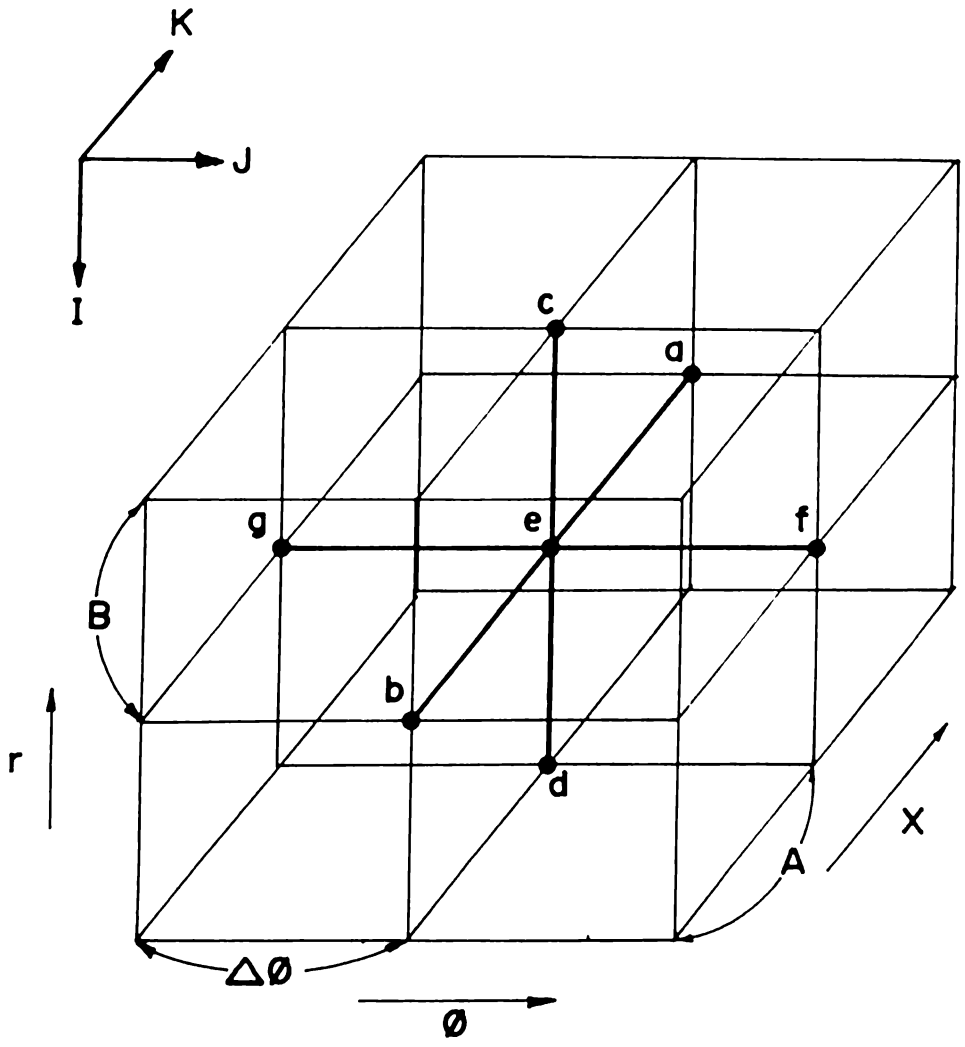

Fig. C. Three dimensional mesh system

$$U_e^{n+1} - U_e^n = C_1 \, (U_c^{n+1} - U_d^{n+1} + U_c^n - U_n^d) \; +$$

$$C_2 \, (V_f^{n+1} - V_g^{n+1} + V_f^n - U_d^n) \; +$$

$$C_3 \, (U_a^{n+1} - U_b^{n+1} + U_a^n - U_b^n) + C_4 \, (P_c^n - P_d^n) \; +$$

$$C_5 \, (U_f^{n+1} + 2U_e^{n+1} + U_g^{n+1} + 2U_e^n + U_g^n)$$

The above equation could be rewritten:

$$U_e^{n+1} = \frac{1}{(1-2C_5)} \left[C_1 (U_c^{n+1} - U_d^{n+1}) + C_2 (V_f^{n+1} - V_g^{n+1}) + C_3 (U_a^{n+1} - U_b^{n+1}) + C_5 (U_f^{n+1} + U_g^{n+1}) + d_e^n \right] \quad (30)$$

where

$$d_e^n = C_1 (U_c^n - U_d^n) + C_2 (V_f^n - V_g^n) + C_3 (U_a^n - U_b^n) + C_4 (P_c^n - P_d^n) + C_5 (U_f^n + 2U_e^n + U_g^n)$$

The iteratione form of Eq. (30) is written:

$$U_e^{p+1} = \frac{1}{(1-2C_5)} \left[C_1 (U_c^{p+1} - U_d^p) + C_2 (V_f^p - V_g^{p+1}) + C_3 (U_a^p - U_b^{p+1}) + C_5 (U_f^p + U_g^{p+1}) + d_e^n \right]$$

where p stands for the iteration number.

The above procedure is called the Gause-Sieded or unextropolated Liebmann's method. The SOR is a modification of the above method, and is written:

$$U_e^{n+1} = U_e^n + \Omega D_e^p \quad (32)$$

where

$$D_e^p = \frac{1}{(1-2C_5)} \left[C_1 (U_c^{p+1} - U_d^p) + C_2 (V_f^p - V_g^{p+1}) + C_3 (U_a^p - U_b^{p+1}) + C_5 (U_f^p + U_g^{p+1}) - (1-2C_5) U_e^p + d_e^n \right]$$

The relaxation factor Ω is usually greater than 1. When $\Omega<1$, it is called successive under-relaxation. When $\Omega = 1$, SOR becomes the Gauss-Siedel method.

Iterative Procedure

Because of symmetry, it is sufficient to solve the problem in one-half of the circular region such as that shown in Fig. A. A 26x27x26 (r,ϕ,X) mesh system is used.

Procedure in Brief

Briefly the solution consists of the following main steps:

1. Determination of the maximum value of the time step size $\Delta\tau$.
2. Determination of the values of the relaxation factor which would give the fastest rate of convergence for the pressure, velocity, and temperature solutions.
3. Iterations for pressure values, until sufficiently convergent.
4. Iterations for the velocities, until sufficiently convergent.
5. Iterations for temperature values, until sufficiently convergent.
6. Steps 3 to 5 are repeated until steady-state profiles are obtained.

Procedure in Detail

This research made use of Miyakoda's method [7], wherein the derivative boundary condition

$$P^{p+1}_{I,J,K} = P^{p+1}_{I+1,J,K} + \frac{\partial P}{\partial r}\,\Delta X$$

is incorporated directly into the SOR differencing scheme at interior points adjacent to the wall, and ordinary SOR for node points more than one node from the wall. After the convergence criterion is satisfied, the wall values are computed using Eq. (33) with $\frac{\partial P}{\partial r}$ as defined in Eq. (27). In a similar way for the computation of values at node points adjacent to the infinite end, the derivative boundary conditions are incorporated into the SOR scheme.

At $\phi = \frac{\pi}{2}$, $r = O$, and because of symmetry, the pressure gradient $\frac{\partial P}{\partial r} = O$. If this gradient is defined in finite-difference form as

$$\frac{\partial P}{\partial r} = \frac{P_{26,14,K} - P_{25,14,K}}{\Delta r}$$

then the approximation as the center would then be:

$$P(26,J,K) = P(25,14,K)$$

The term in Eq. (23) which contain the derivative $\frac{\partial D}{\partial \tau}$ where $D = \frac{\partial U}{\partial r} + \frac{1}{r}\frac{\partial V}{\partial \phi} + \frac{\partial W}{\partial X}\frac{dX}{dx}$, could have easily been cancelled out with

the continuity equation, Eq. (18). But due to incompatible initial conditions or of incomplete solution of the Poisson equation, the finite difference $\frac{D^{n+1} - D^{n}}{\Delta t}$ is not equal to zero. Successful studies [6] had been conducted which retained $\frac{\partial D}{\partial t}$. Its inclusion in the Poisson equation could eliminate nonlinear instability in the momentum equations. When steady-state conditions shall have been attained, D^{n+1} becomes zero. So, $\frac{\partial D}{\partial t}$ is included which is evaluated by forward-time differencing. Therefore

$$\frac{\partial D}{\partial t} = -\frac{D^{n}}{\Delta t} .$$

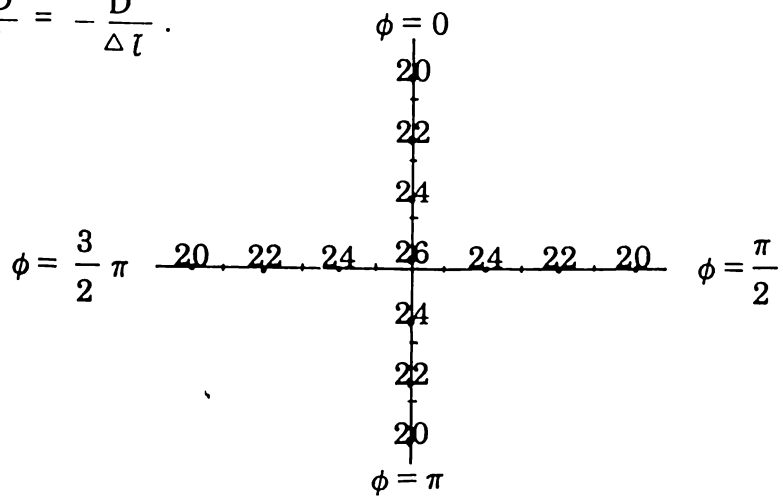

Fig. D

From Fig. A, the velocity at the center is given by the relationship $U_{\phi = o} = V_{\phi = \frac{\pi}{2}} = U_{\phi = \pi}$. To ensure that this relationship is retained in the finite-difference solution, a method is introduced. The values of U,V, and W at points 20-24 (Fig. D) are first changed into u.v, and w according to Eq. 16). Then the average of the Taylor series expansions for $\phi = o, \frac{\pi}{2}, \pi, \frac{3\pi}{2}$ is used to approximate the value at the center:

$$u_{26} = \frac{1}{4}\left[(3u_{24} - 3u_{22} + u_{20})_{\phi = o} + 2\,(3v_{24} - 3v_{22} + v_{20})_{\phi = \frac{\pi}{2}, \frac{3\pi}{2}} + (3u_{24} - 3u_{22} + u_{20})_{\phi = \pi} \right]$$

Then with this value for u at the center, all values of u and v at node points adjacent to the center are corrected by Taylor series expansion using points 23,24, and 26. With reference to Figs. A and D:

$$u(25,J,K) = \frac{1}{3}\left[u(26,1,K)\,(\cos\phi) + 3u\,(24,J,K) - u\,(23,J,K) \right]$$

$$v(25,J,K) = \frac{1}{3}\left[-u(26,1,K)\,(\sin\phi) + 3v\,(24,J,K) - v\,(23,J,K) \right]$$

This method of approximating the velocities at the center and the subsequent corrections for the node points adjacent to the center has been found to give more stable results.

Approximation for the values of temperature at the center is done by taking the average of the Taylor series expansions for $\phi = 0$, and $\phi = \pi$. With reference to Fig. D:

$$\theta_{26} = \frac{1}{2}\left[(3\theta_{25} - 3\theta_{24} + \theta_{23})\ \phi = 0 + (3\theta_{25} - 3\theta_{24} + \theta_{23})\ \phi = \pi\right]$$

With the above approximations and SOR differencing scheme for the governing equations, the maximum value for the time-step size $\Delta\tau$ is determined. Trial computations are made with the relaxation factor $\Omega = 1$ for the pressure, velocity, and temperature equations. After a careful study of the behavior of the results, the time-step size is fixed. With this value for $\Delta\tau$, trial computations are made to determine the maximum values of Ω which would give the fastest rate of convergence for the pressure, velocity, and temperature solutions.

With initial values obtained from laminar pure forced convection, pressure values are evaluated until the convergence criterion is satisfied. With the new values of P, the velocities are computed until convergent. The temperatures are then solved, and when convergent, the computations would continue with the next time level. The computations end when the desired number of time-iterations shall have been reached.

Local and average Nusselt numbers are obtained by:

$$\text{Average: } \overline{Nu} = -\frac{2}{\pi\,\theta_b}\int_0^{\pi}\left.\frac{\partial\theta}{\partial r}\right|_{r=1} d\phi$$

$$\text{Local: } Nu = -\frac{2}{\theta_b}\left.\frac{\partial\theta}{\partial r}\right|_{r=1} \qquad \text{where } \theta_b = \frac{\int_A w\,\theta\,dA}{\int_A w\,dA}$$

The convergence criterion is given by:

$$\frac{\max.\left|X^{p} - X^{p+1}\right|}{\max.\left|X^{p+1}\right|} < \epsilon$$

where X stands for the parameters U,V,W,P, and Temp., as the case may be.

$\epsilon = 0.001$ for the pressue.

$\epsilon = 0.00001$ for the velocities and temperature.

Other assumed values are:

Re = 100, Gr = 5000, Pr = 0.71 (air)

For Eq. (17):

c = 30, m = 0.95

Results and Discussion

Accuracy and Convergence

The "p" Loop

The governing equations contain nonlinear terms so that existing stability analyses to compute for the time-step size could not be applied. Trial computations were then used. A time-step size of $\Delta\tau = 0.0001$ was found to be the maximum value with which the whole finite-differencing scheme was stable. The pressure equation determined this restrictive stability requirement. With this value for $\Delta\tau$, the relaxation factor Ω for the pressure, velocity, and temperature equations were determined. A value of $\Omega = 1.86$ for the pressure, and $\Omega = 1.0$ for the velocity and temperature equations, were found to give the fastest rate of convergence. The convergence criterion $\varepsilon = 0.001$ for the pressure, and $\varepsilon = 0.00001$ for the velocities and temperature, were satisfied for every time step after about twelve iterations for the temperature, fourteen for the velocities, and forty-three for the pressure. A faster rate of convergence of the pressure values was achieved (about four times faster) when ordinary centered-space differencing was used for the pressure derivatives in the pressure loop instead of Euler's and Grank-Nicolson's methods.

The Time Loop

After two-hundred sixty time-iterations, the solution was believed to have attained steady-state convergence. The rate of convergence is illustrated in the Appendix, with time-iterations 40, 80, 140, 200, and 260.

Velocity Field Characteristics

Although the determination of the local and average Nusselt numbers is of primary importance in many industrial applications, the growth and decay of the secondary flow and its effect on the developing main flow are also of great engineering importance. To study the effect of the secondary flow, it is necessary to make a comparison of results obtained in this research with those of pure forced convection.

The developing velocity profiles for pure forced convection are shown in Figs. 1 and 2, while those obtained here are shown in Figs. 3, 4, and 5. The velocity profiles are illustrated using axial location as parameter; and for convenience in the discussion, letters are used.

Comparison of the velocity profiles marked A in Figs. 1 and 3 reveals that the value of the axial velocity w in the central region are larger for the combined flow. With the same axial location A, a comparison of the profiles for the velocity component u, shown in Figs. 2 and 4, reveals that the values for the combined flow are smaller. The theory of conservation of mass and momentum then suggests that the gain in the axial velocity of the combined flow (relative to the axial velocity of pure forced flow) is a response to the loss in the transverse velocity. To study the relationship, the velocity profiles at

the downstream location marked B are presented for analysis. Comparison of values at the central region shows that the axial velocity decreased, and the secondary velocity component u increased, relative to those of pure forced flow. A careful study of the velocity profiles at other axial locations also indicate the same relationship between axial velocity and secondary flow. Further insight into the understanding of the effect of free convection could be obtained from flow visualizations shown in Figs. 6-9. Secondary velocity vectors are plotted for the four axial locations A, B, D, E. Figure 6 shows the birth of the secondary flow. It gradually develops downstream as the warmer fluid near the wall moves upward and the cooler fluid at the core moves downward, as shown in Fig. 7. It attains its maximum intensity at the axial location D, Fig. 8, and then gradually decreases as the fluid moves further downstream, Fig. 9. The movement of the eye of the vortex is also of interest. It starts from the lower region and moves upward with some movement toward the center. The upward movement is correlated to the upward movement of the peak points of the axial velocity as observed in Fig. 3b. The movement toward the center is correlated to the horizontal movement (toward the center) of the peak point of the axial velocity, as can be observed in Fig. 3a. It is of interest to note that the eye of the secondary flow is the region where the intensity is minimum. The above observations support the hypothesis that the secondary flow affects the main flow in an inverse relationship.

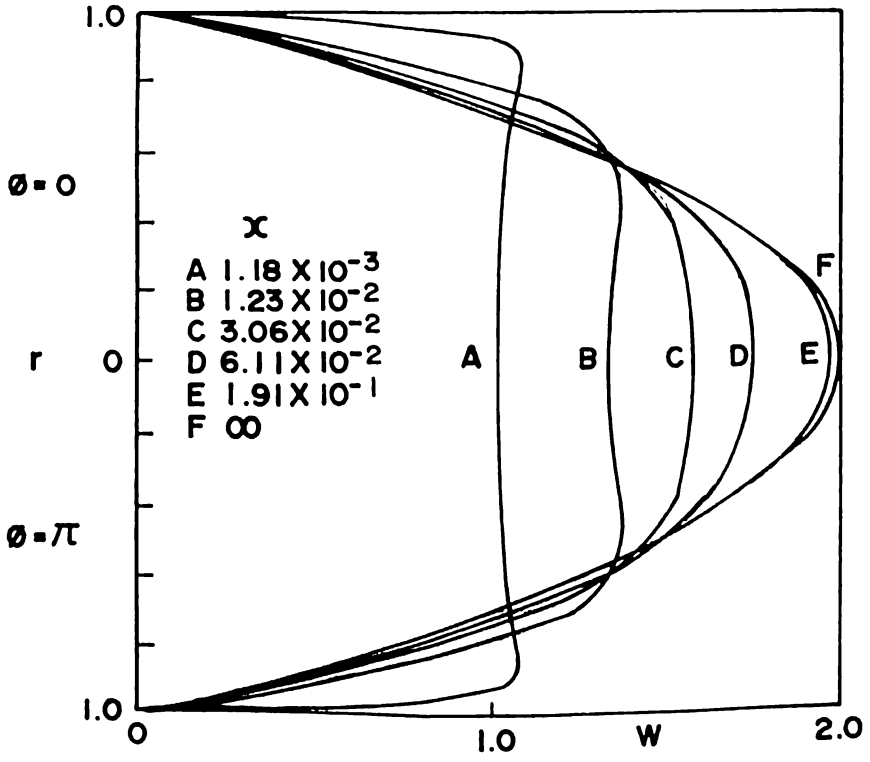

FIG. 1. Development of axial velocity profiles along the vertical center line for Gr = 0.

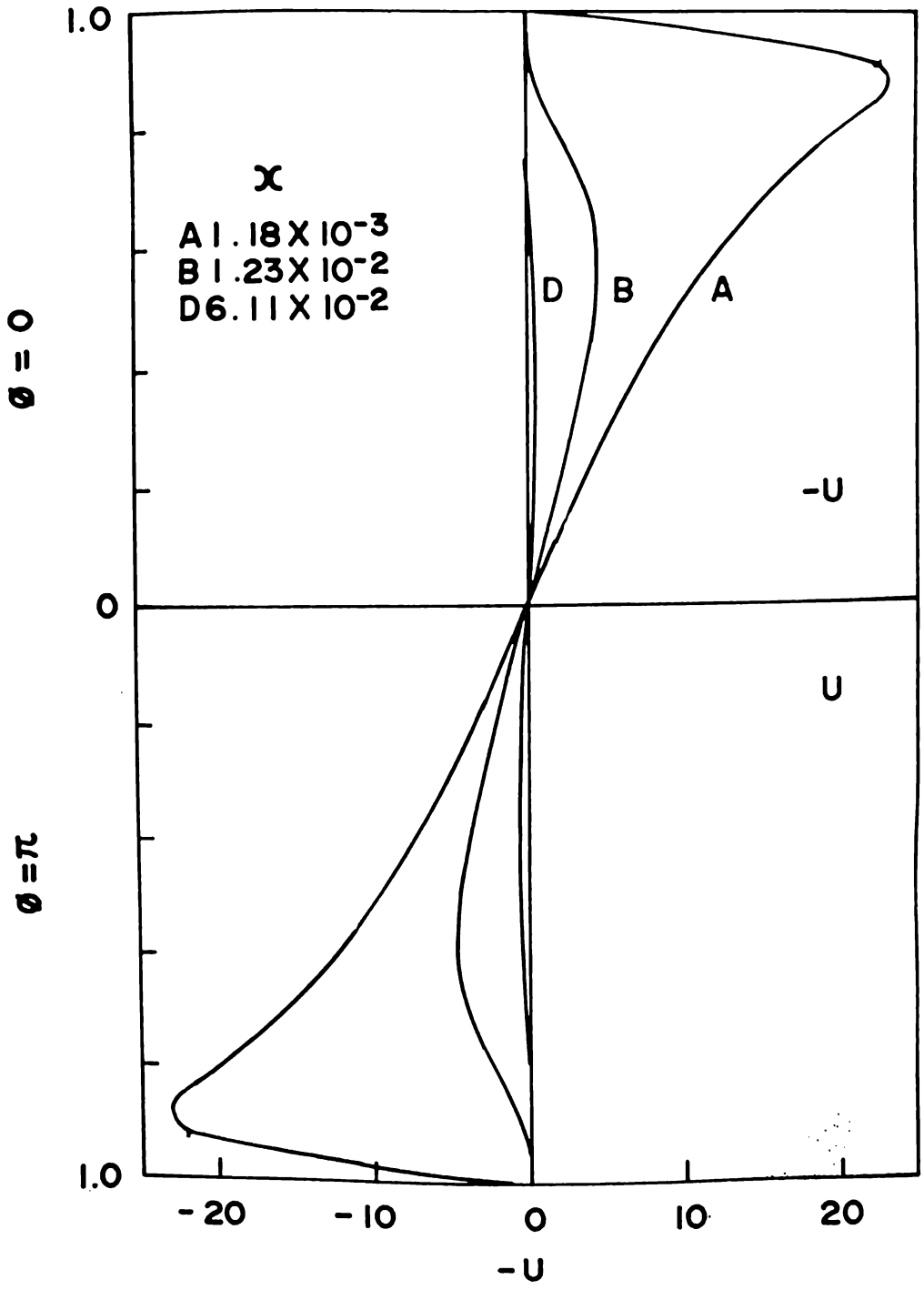

FIG. 2. Development of velocity profiles of the velocity component u along the horizontal center line for Gr = 0.

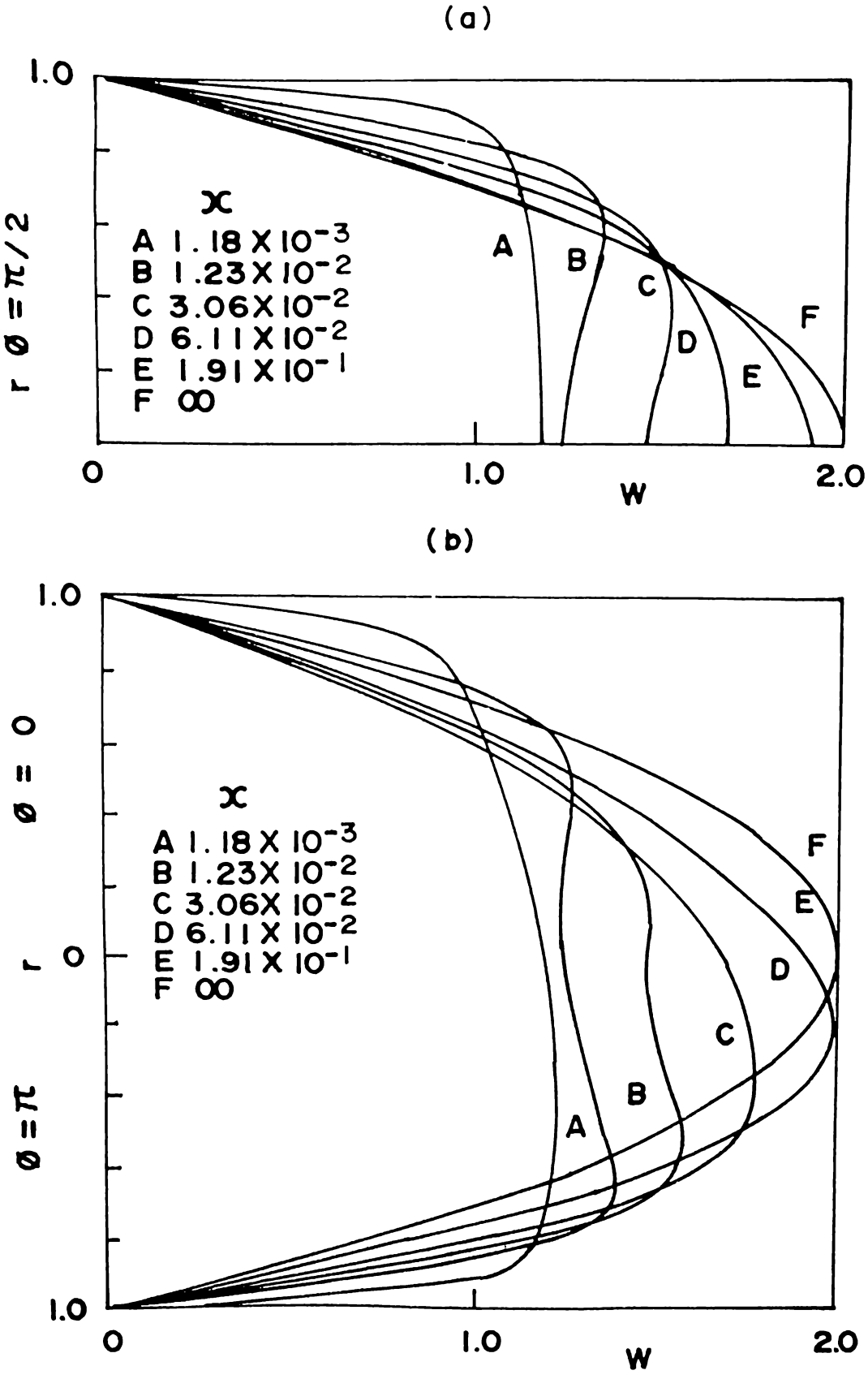

FIG. 3. Developing axial velocity profiles along (a) horizontal center line (b) vertical center line.

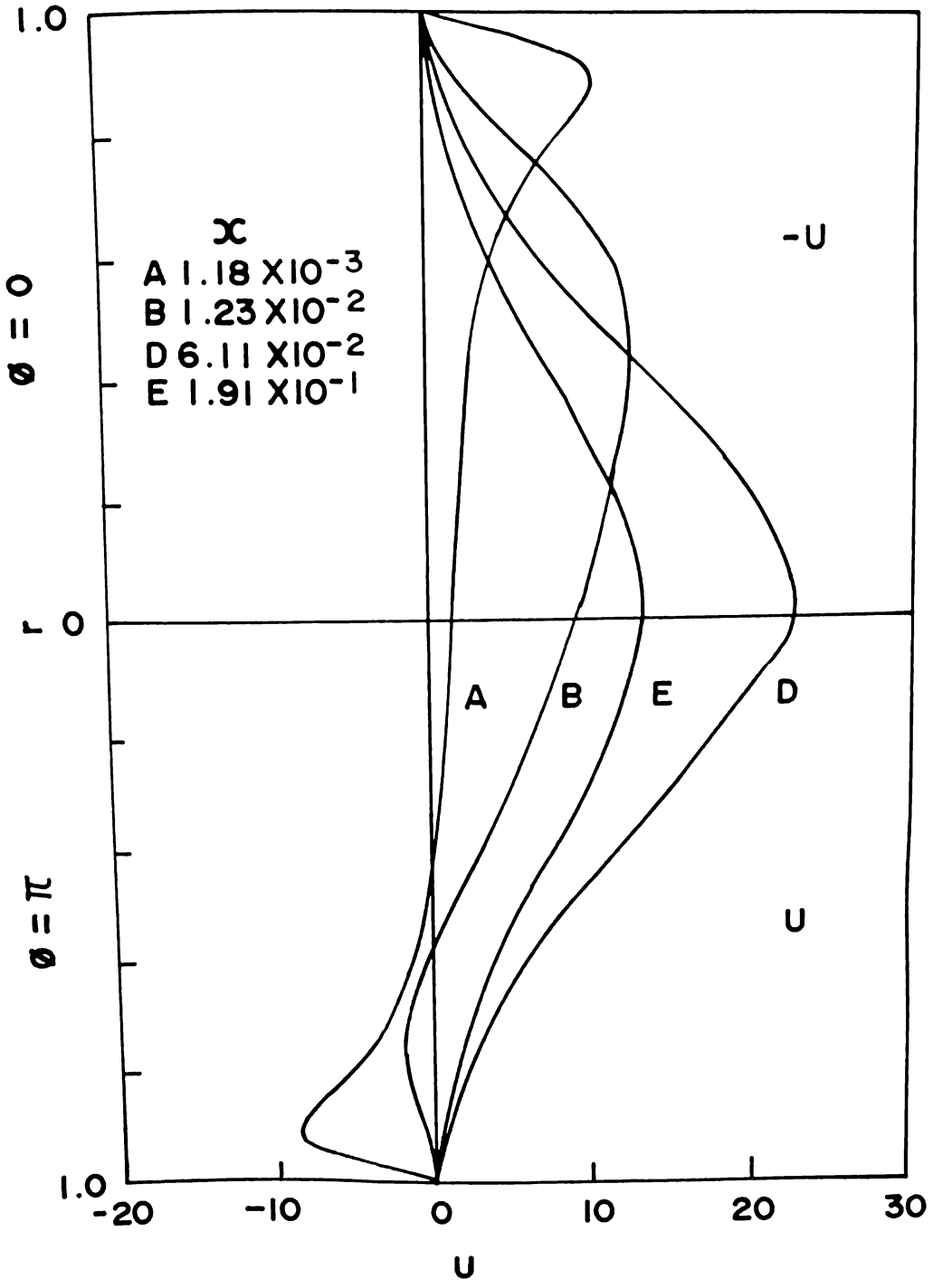

FIG. 4. Development of the secondary velocity profiles of the component u along the vertical center line.

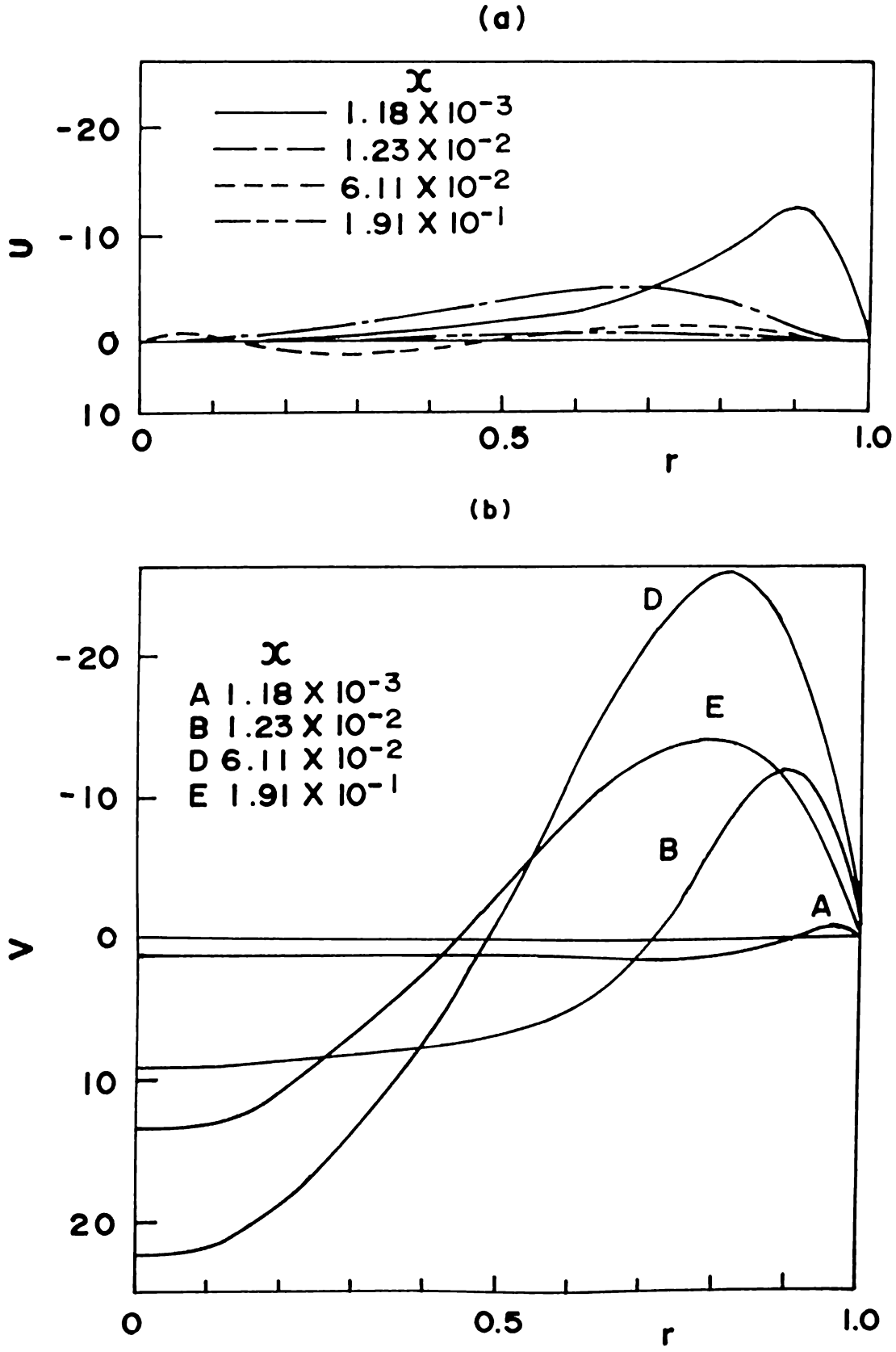

FIG. 5. Development of the secondary velocity profiles along the horizontal center line (a) velocity component u (b) velocity component v.

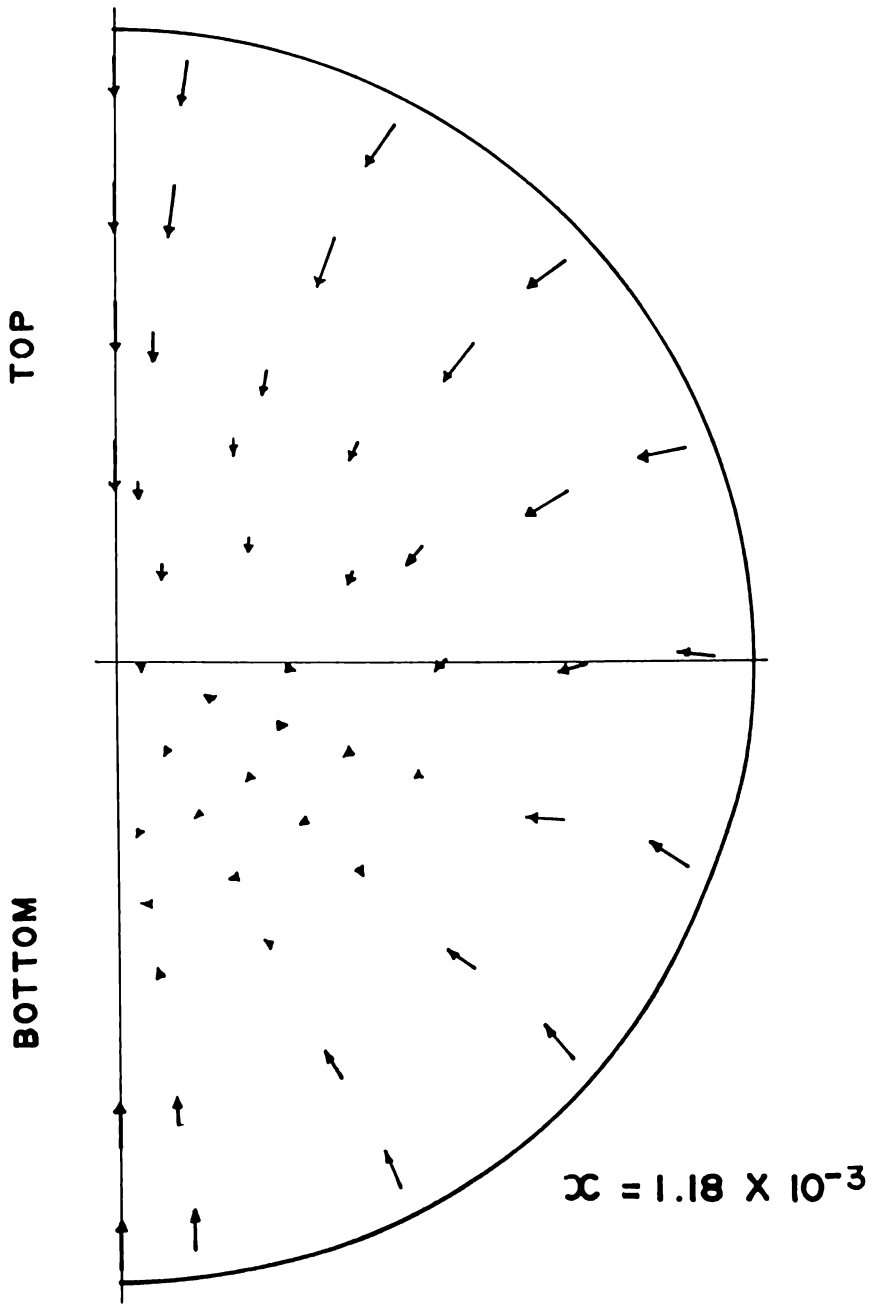

FIG. 6. Secondary velocity vector flow pattern at the axial location x = 0.00118.

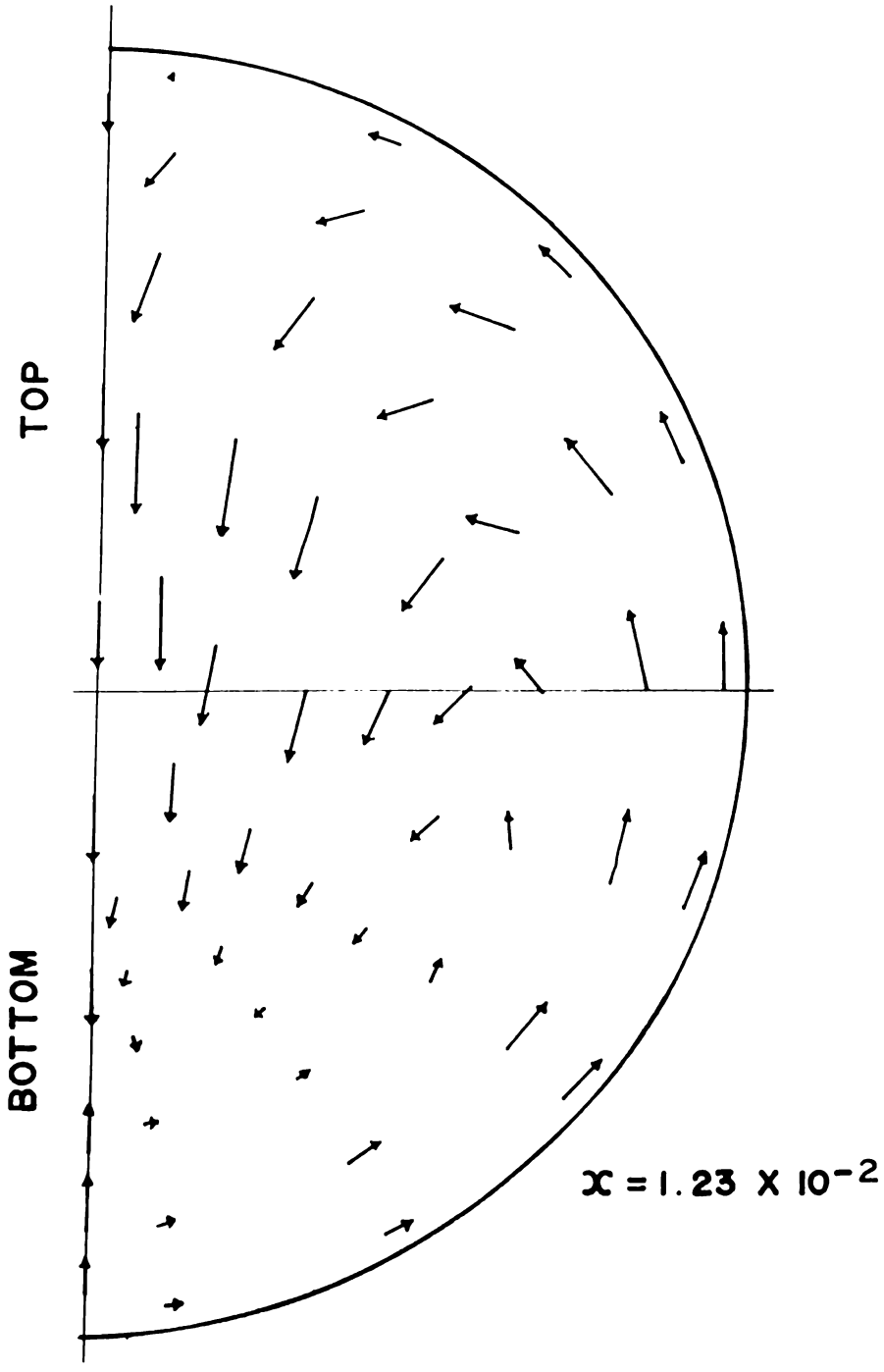

FIG. 7. Secondary velocity vector flow pattern at the axial location x = 0.0123.

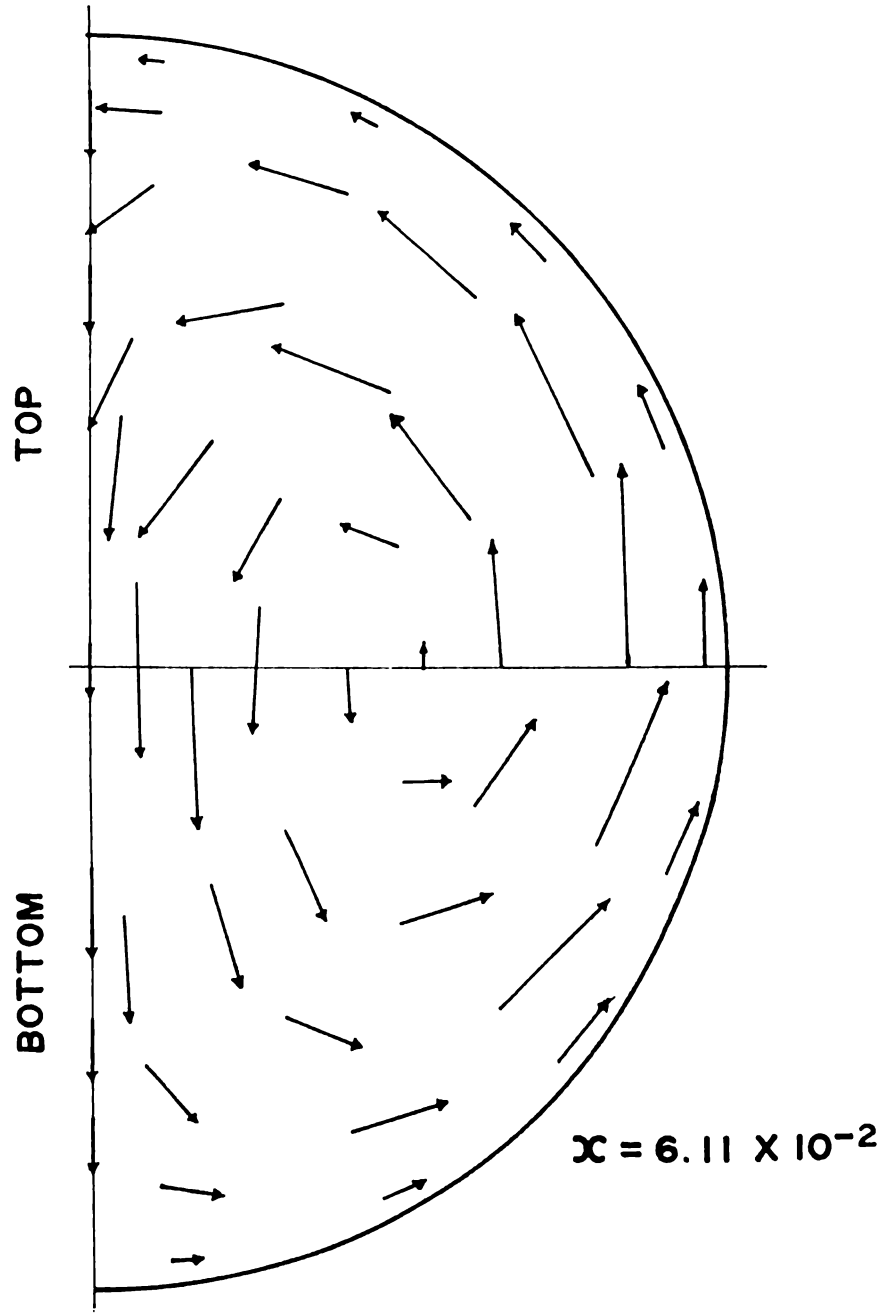

FIG. 8. Secondary velocity vector flow pattern at the axial location x = 0.0611.

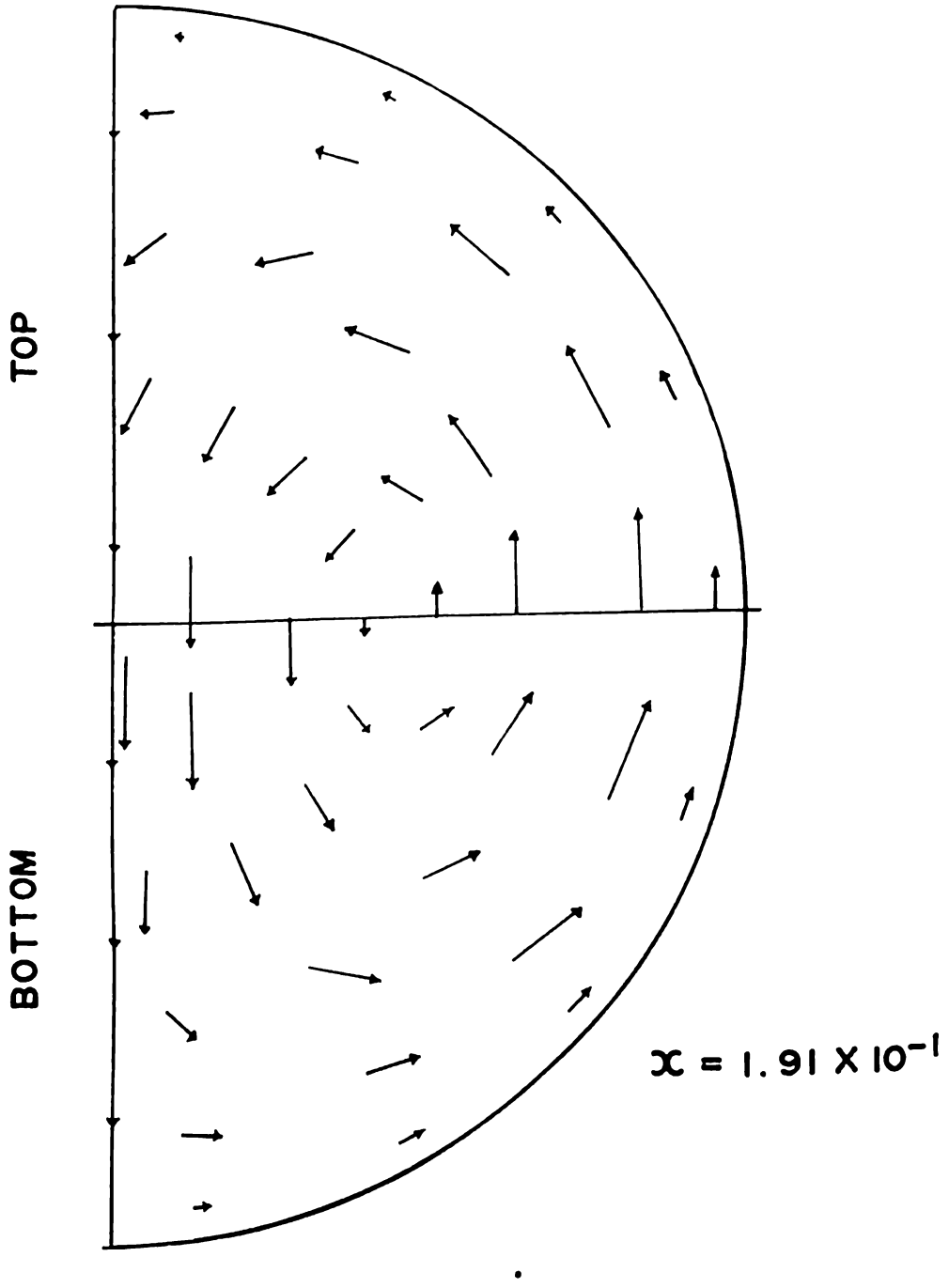

FIG. 9. Secondary velocity vector flow pattern at the axial location x = 0.191.

TEMPERATURE FIELD AND NUSSELT NUMBER

The temperature profile is of interest in the study of the local Nusselt number behavior. It can be seen from Fig. 11 that the normal temperature gradients are greater in the lower region than in the upper region of the pipe. (The developing temperature profiles for pure forced flow is shown in Fig. 10 for reference). This is expected because in the upper region the warmer fluid near the wall is constantly transported upward, while on the other hand, near the bottom of the pipe, the cooler fluid in the core region is continually transported downward. Consequently, the local Nusselt numbers are smaller in the upper region and larger in the lower region. The variations of the local Nusselt number are shown in Figs. 13 and 14. A "dip" in the curves for B, D, and E near $\phi = \tau$ is observed in Fig. 14. This could perhaps be due to some form of "stagnation" caused by the interaction of the downward flow from the core region and the rising fluid from the bottom part of the wall. Further study is deemed necessary to clarify this matter.

Some insight may be gained by contrasting the velocity profiles shown in Figs. 4 and 5 with the local Nusselt number variations in Figs. 13 and 14. At the axial location D, the intensity of the secondary flow is at its peak. This same axial location ($x = 0.0611$) corresponds to where the maximum variations of the local Nusselt number occur.

Higher average Nusselt number values are obtained in this research as compared with those obtained from pure forced convection. The comparison is shown in Fig. 12. The thermal entrance length for the combined flow is longer than that of pure forced convection by about 1.35 pipe diameters. This result was obtained with the assumption that the entry length extends up to the point where the value of the average Nusselt number has come one per cent close to the value at infinity ( ). Significant variations (2 per cent minimum) of the local Nusselt numbers are observed as far as 17.5 pipe diameters. It is interesting to note (Figs. 13 and 14) that the average Nusselt numbers are almost identical with the local Nusselt numbers at $\phi =$ (maximum difference of about 2.5 per cent).

The limiting value of $Nu_\infty = 3.66$ is approached asymptotically.

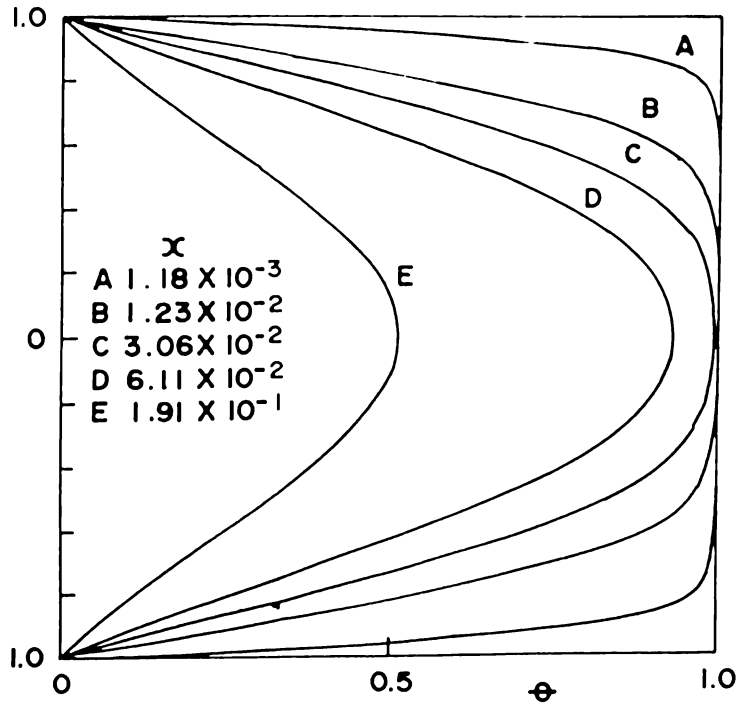

FIG. 10. Development of the temperature profiles along the vertical center line for Gr = 0

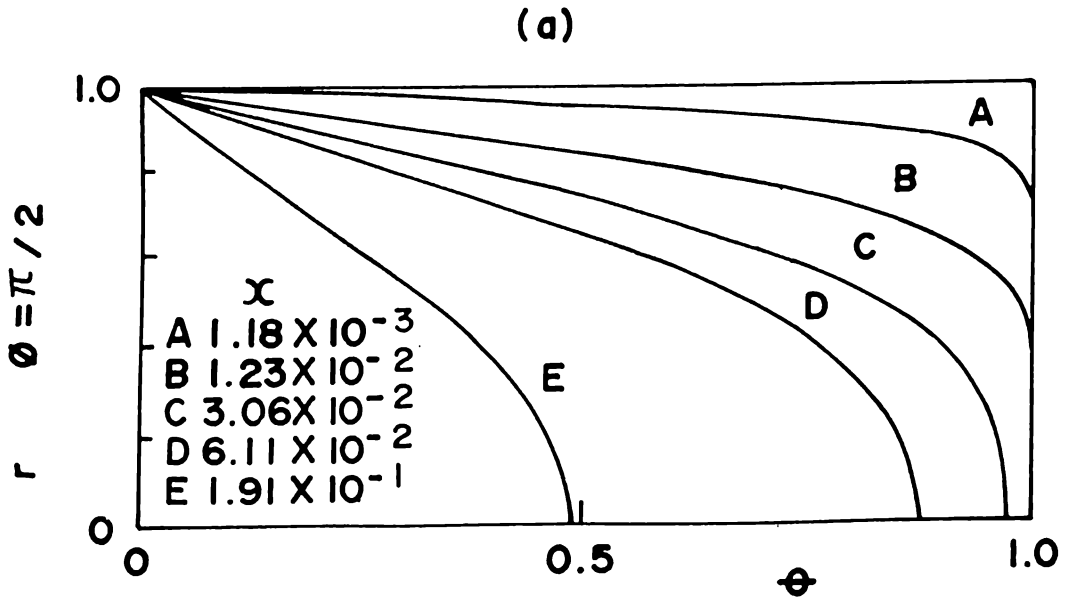

FIG. 11. Development of temperature profiles along (a) horizontal center line

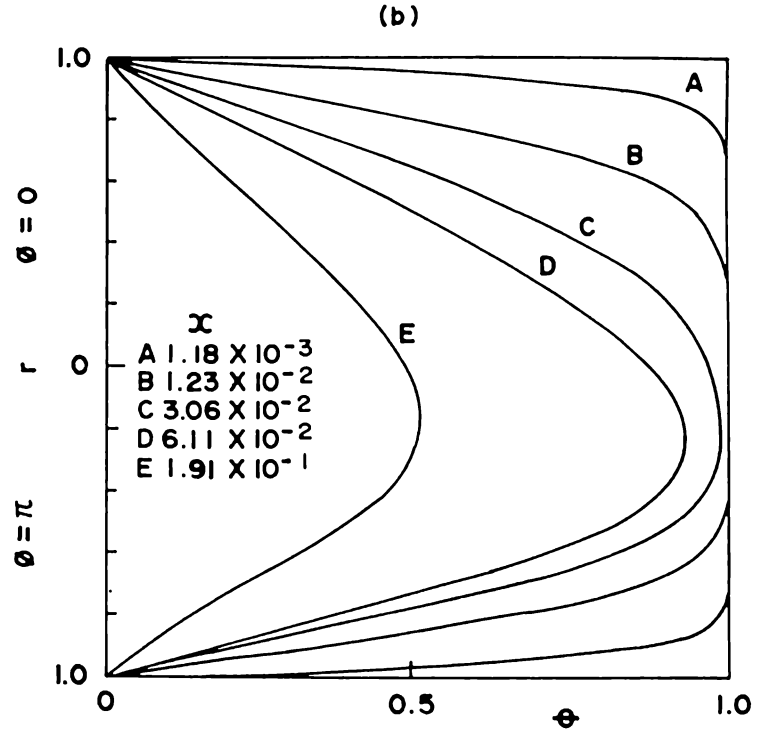

(b) vertical center line

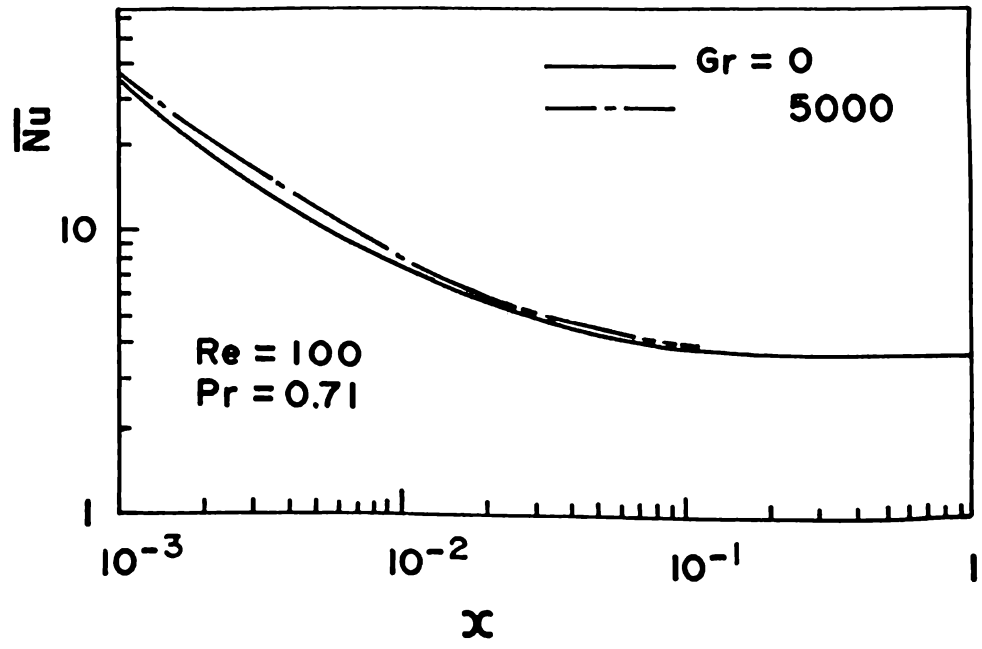

FIG. 12. Average Nusselt number values for Gr = 0 and Gr = 5000

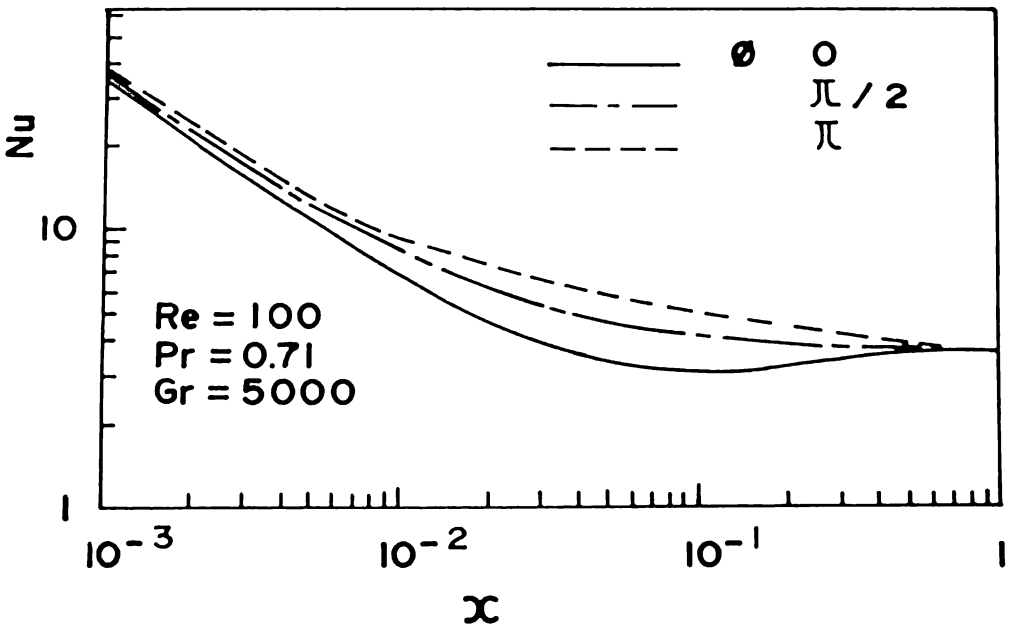

FIG. 13. Local Nusselt number variations at locations $\phi = 0,$, π

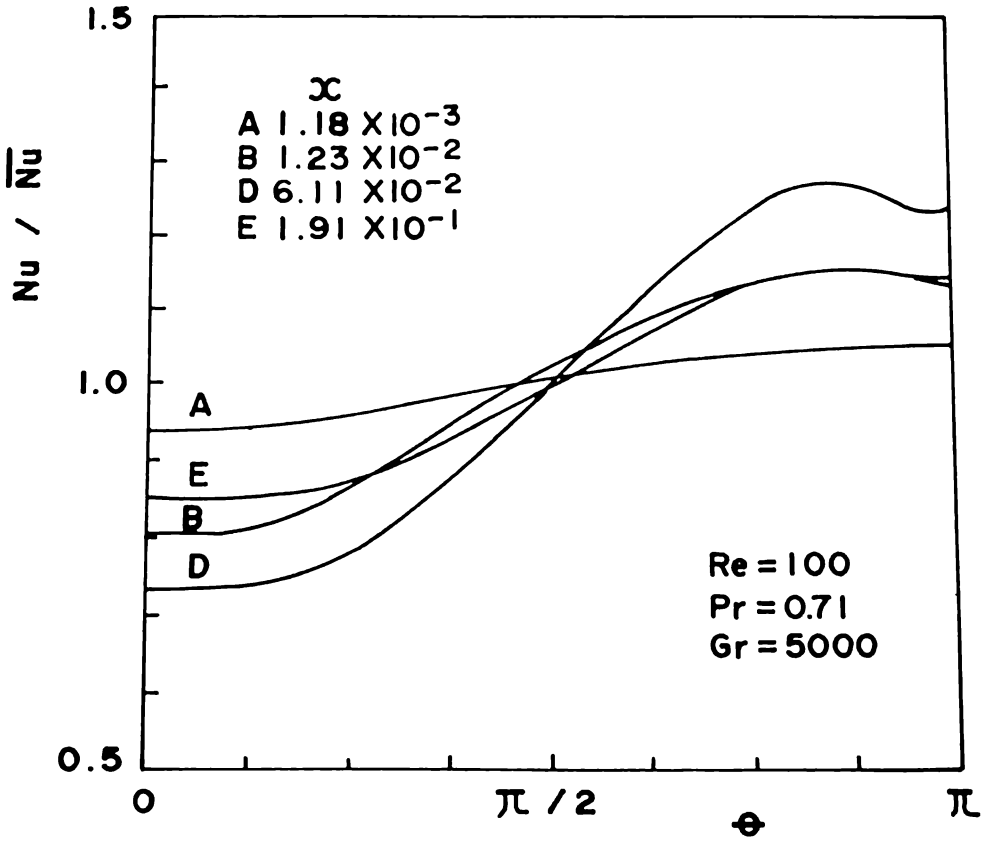

FIG. 14. Deviations of the local Nusselt numbers from the average

SUMMARY AND CONCLUSION

A novel iterative finite-differencing scheme has been developed to solve nonlinear partial differential equations. It has been found stable and faster rate of convergence has been achieved.

The secondary flow not only distors the parabolic development of the axial flow, but also considerably increases the thermal entrance length.

Significant variations of the local Nusselt numbers are observed as far as 17.5 pipe diameters, and the average values are higher compared with those obtained from pure forced convection. The limiting value of $Nu_\infty = 3.66$ is approached asymptotically.

A direct comparison of the present results with those of other investigations [2-4] is not possible due to the major difference in the assumptions.

The present problem is one of the basic convective heat-transfer problems, and the results obtained are helpful in the understanding of the complex phenomena which occur when the velocity and temperature fields are developing simultaneously. Furthermore, the results are applicable to low Prandtl number fluids for which the results obtained from large Prandtl number assumptions are no longer valid.

NOMENCLATURE

Symbol	*Description*
Cp	Specific heat
g	Acceleration due to gravity
p'	Pressure
r'	Radial distance from the pipe center
r'_o	Inside radius of the pipe
t'	Fluid temperature
t'_o	Fluid temperature at the pipe inlet
t'_w	Wall temperature
u'	Radial velocity component
v'	Tangental velocity component
w'	Axial velocity component
w'_o	Fluid velocity at the pipe inlet
x'	Axial coordinate
α	Heat transfer coefficient
β	Coefficient of volumetric expansion
κ	Thermal conductivity, $(\lambda/\rho\ Cp)$
λ	Heat transfer coefficient for conduction
ν	Kinematic viscosity
ρ	Density
ρ_w	Fluid density at the wall
ϕ	Angle measured clockwise from the upper vertical centerline; radians
τ'	Time
$\Delta\tau'$	Time increment

Dimenssionless numbers

Ω	Relaxation facor for the pressure, velocity, or temperature SOR differences scheme
A	Axial increment in the finite-difference approximation
B	Radial increment in the finite-difference approximation
c	Constant in Eq. (17)
Gr	Grashof number, $(\beta g r_o'^3 (t_w'-t_o') /\nu^2)$
m	Constant in Eq. (17)
Nu	Nusselt number, $(2r_o'\alpha/\lambda)$
P	Pressure
Pr	Prandtl number, (ν/κ)
Re	Reynolds number, $(2r_o'w_o'/\nu)$
r	Radius, (r'/r_o)
u	Radial velocity component, $(Reu' /2w_o')$
v	Tangental velocity component, $(Rev'/2w_o')$
w	Axial velocity component, (w'/w_o')
U,V,M,	Transformations of u,v,w from Eq. (16)
x	Axial coordinate, $(2x'/r_o' Re)$
X	Transformation of x from Eq. (17)
θ	Temperature, $(t'-t_w')/(t_o'-t_w')$
θ_b	Bulk temperature, $(w\theta dA / wdA)$
$\Delta\phi$	Angular increment in the finite-difference approximation
$\Delta\tau$	Time increment in the finite-difference approximation

Subscripts

a,b,c, d,e,f,g	Node points used in the presentation of the finite-difference scheme, Fig. C

Superscripts

n	Time-loop iteration number
p	Pressure, velocity, or temperature-loop iteration number
—	Average